Climate
of the Past
Open Access
Discussions
EGU

1 **Oligocene–Miocene paleoceanography off the Wilkes Land Margin**

2 **(East Antarctica) based on organic-walled dinoflagellate cysts**

3

4 Peter K. Bijl[1]*, Alexander J. P. Houben[2], Julian D. Hartman[1], Jörg Pross[3], Ariadna

5 Salabarnada[4], Carlota Escutia[4], Francesca Sangiorgi[1]

6

7 1 Marine Palynology and Paleoceanography, Laboratory of Palaeobotany and

8 Palynology, Department of Earth Sciences, Faculty of Geosciences, Utrecht University.

9 P.O. Box 80.115, 3508 TC Utrecht, The Netherlands

10

11 2 Applied Geoscience Team, Netherlands Organisation for Applied Scientific Research

12 (TNO), Princetonlaan 6, 3584 CB, Utrecht, The Netherlands

13

14 3 Paleoenvironmental Dynamics Group, Institute of Earth Sciences, University of

15 Heidelberg, Im Neuenheimer Feld 234, 69120 Heidelberg, Germany

16

17 4 Instituto Andaluz de Ciencias de la Tierra, CSIC-UGR, 18100 Armilla, Spain

18

19 * to whom correspondence should be addressed.

20 Email: p.k.bijl@uu.nl; phone +31 30 253 9318

21

22 **Abstract**

23 **Next to atmospheric CO_2 concentrations, oceanographic conditions are a critical**

24 **factor determining the stability of Antarctic marine-terminating ice sheets. The**

25 **Oligocene and Miocene epochs (~34–5 Ma) were time intervals with**

26 **atmospheric CO_2 concentrations between those of present-day and those**

27 **expected for the near future. As such, these time intervals may bear**

28 **information to resolve the uncertainties that still exist in the projection of**

29 **future ice-sheet volume decline. We present organic-walled dinoflagellate cyst**

30 **(dinocyst) assemblages from chronostratigraphically well-constrained**

31 **Oligocene to mid-Miocene sediments from Integrated Ocean Drilling Program**

32 **Expedition (IODP) Site U1356. Situated offshore the Wilkes Land continental**

33 **margin, East Antarctica, the sediment core has archived past dynamics of an ice**

34 **sheet that is today mostly grounded below sea level. We interpret dinocyst**

35 **assemblages in terms of paleoceanographic change on different time scales, i.e.,**

36 **on glacial-interglacial and long-term variability. Sea-ice indicators occur only**

37 **for the first 1.5 Ma following the full Antarctic continental glaciation during the**

38 **early Oligocene, and after the Middle Miocene Climatic Optimum. During the**

39 **remainder of the Oligocene and Miocene dinocysts suggest a weaker-than-**

40 **modern sea-ice season. The assemblages generally bear strong similarity to**

41 **present-day open-ocean, high-nutrient settings north of the sea ice edge, with**

42 **episodic dominance of temperate species similar to the present-day subtropical**

43 **front. Oligotrophic and temperate surface waters prevailed over the site**

44 **notably during interglacial time intervals, suggesting that the position of the**

Climate
of the Past

Open Access

EGU

Discussions

45   **(subpolar) oceanic frontal systems have varied in concordance with Oligocene-**

46   **Miocene glacial-interglacial climate variability.**

47

48   **1. Introduction**

49   The proportion of the East Antarctic ice sheet that is presently grounded

50   below sea level is much larger than originally assumed (Fretwell et al., 2013). This

51   implies that much more ice is sensitive to basal melting by warm waters than

52   previously thought (Shepherd et al., 2012; Rignot et al., 2013; Wouters et al., 2015),

53   and that a much higher amplitude and faster rate of sea-level rise under future

54   climate scenarios than previously thought (IPCC, 2013). Studying the state and

55   variability of Antarctic ice volume during past episodes with high atmospheric CO_2

56   concentrations (pCO$_2$) might provide additional understanding into ice/ocean

57   feedback processes. Foster and Rohling (2013) compared sea-level and atmospheric

58   pCO$_2$ concentrations on geological timescales and highlighted that global ice sheets

59   were rather insensitive to climate change under atmospheric pCO$_2$ between 400 and

60   650 parts per million in volume (ppmv). During the Oligocene and Miocene

61   atmospheric pCO$_2$ ranged between 400 and 650 ppmv (Foster et al., 2012; Badger et

62   al., 2013; Greenop et al., 2014). Crucially, similar pCO$_2$ levels are expected for the near

63   future given unabated carbon emissions (IPCC, 2013), implying that global ice volume

64   may not change much under these pCO$_2$ scenarios.

65   In contrast to the invariant global ice volume inferred by Foster and Rohling

66   (2013), a strong (up to 1 per mille; ‰) variability is observed in deep-sea benthic

67   foraminiferal oxygen isotope (hereafter benthic δ^{18}O) data (Pälike et al., 2006;

68   Beddow et al., 2016; Holbourn et al., 2007; Liebrand et al., 2011; 2017). These

69   benthic $\delta^{18}O$ data reflect changes in continental ice volume (notably on Antarctica), in

70   combination with deep-sea temperature, with the latter strongly coupled to polar

71   surface-water temperature, as deep-water formation was predominantly located at

72   high latitudes (Herold et al., 2011). High-amplitude variations in benthic $\delta^{18}O$ thus

73   suggest either (I) strong climate dynamics in the high latitudes with relatively minor

74   ice-volume change (which is in accordance with numerical modelling experiments

75   (Barker et al., 1999) and the inferences of Foster and Rohling (2013)), or (II) strong

76   fluctuations of the Antarctic ice-volume, with relatively subdued temperature

77   variability (which is in accordance with indications for an unstable Antarctic ice

78   sheets under warmer-than-present climates (Cook et al., 2013; Greenop et al., 2014;

79   Rovere et al., 2014). Indeed, if one assumes present-day δ-composition (-42‰ versus

80   standard mean ocean water (SMOW)) for the Oligocene–Miocene Antarctic ice-sheets

81   and modern deep water temperature (2.5°C), then the Oligocene–Miocene benthic

82    $\delta^{18}O$ fluctuations suggest long-term ice-sheet-variability ranging between a present-

83   day size for 27–23 Ma and absence during numerous other time intervals (Liebrand

84   et al., 2017). Meanwhile, deep-sea temperatures have fluctuated considerably on

85   geologic time scales (as is evident from ice-free geologic episodes –e.g., Zachos et al.,

86   2008), suggesting there is no reason to assume that it did not fluctuate during the

87   Oligocene or Miocene as well. Therefore, likely a combination of deep-sea

88   temperature and ice-volume changes is represented in these records, but it is

89   intrinsically impossible to determine the relative contribution of both factors from

90   benthic $\delta^{18}O$ data alone. Clearly, ice-proximal reconstructions of climate, ice sheet and

91   oceanographic conditions are required to provide an independent assessment of the

92   stability of ice sheets under these pCO$_2$ conditions.

Climate
of the Past
Discussions

93   While the Oligocene–Miocene may, in terms of pCO$_2$ conditions, bear analogy

94   to our future, any such investigation must take into account the uncertainties

95   involved in Antarctic paleotopography, which determines the proportion of marine-

96   based versus land-based ice during the Oligocene. A lower Antarctic continent would

97   result in more ice sheets being potentially sensitive to basal melt, and as such a

98   higher sensitivity of the ice sheet to climate change. On top of this, one should take

99   note of the fundamentally different paleogeographic configuration of the Southern

100   Ocean during that time as compared to today (Figure 1). The development and

101   strength of the Antarctic Circumpolar Current (ACC) connecting the Atlantic, Indian

102   and Pacific Ocean basins (Barker and Thomas, 2004; Olbers et al., 2004) depend on

103   the basin configuration (width and depth of the gateways and position of continental

104   landmasses). The exact timing when the ACC reached its modern-day strength is still

105   uncertain, ranging from the Middle Eocene (41 Ma) to as young as Miocene (23 Ma,

106   Scher and Martin, 2004; Hill et al., 2013; Scher et al., 2015). Whether, and if so, how

107   the development of the ACC has influenced latitudinal heat transport, ice-ocean

108   interactions and the stability of Antarctic continental ice remains even more elusive.

109   To directly assess the role of ice-proximal oceanography on ice-sheet stability

110   during the Oligocene–Miocene, ice-proximal proxy-records are required. Several

111   ocean drilling efforts in the past have been undertaken to provide insight in the

112   history of the Antarctic ice sheets (Cooper and O'Brien, 2004; Barker et al., 1998;

113   Wise and Schlich, 1992; Barrett, 1989; Robert et al., 1998; Wilson et al., 2000;

114   Harwood et al., 2006; Exon et al., 2004; Escutia et al., 2011a). For some of these

115   sedimentary archives, establishment of age control was particularly challenging due

116   to the paucity of useful and proper means to calibrate the record to the international

117 time scale. As a consequence, their full use for the generation of paleoceanographic

118 proxy records and ice sheet reconstructions has remained limited.

119   In 2010, Integrated Ocean Drilling Program (IODP) Expedition 318 drilled an

120 inshore-to-offshore transect off Wilkes Land (Fig. 1a), a sector of East Antarctica that

121 is assumed to be highly sensitive to continental ice-sheet melt (Escutia et al., 2011b).

122 The sediments recovered from IODP Hole U1356A are from the continental rise of

123 this margin (Escutia et al., 2011b) and hence contain a mixture of shelf-derived

124 material and pelagic sedimentation. Dinoflagellate cyst events in this record have

125 been accurately tied to the international time scale through integration with

126 calcareous nannofossil, diatom and magnetostratigraphic data (Bijl et al., in press).

127 The result is a – for Southern Ocean standards – solid stratigraphic age frame for the

128 Oligocene–Miocene part of the record of Hole U1356 (Fig. 2; Table 1). In this paper,

129 we investigate the dinocyst assemblages from this succession by utilizing the strong

130 relationships between dinocyst assemblage composition and surface-water features

131 of today's Southern Ocean (Prebble et al., 2013). We reconstruct the oceanographic

132 regimes during the Oligocene and mid-Miocene, and speculate on their implications

133 for oceanographic settings. We further compare the palynological data with detailed

134 sedimentological descriptions from Salabarnada et al. (submitted this volume).

135 Pairing the sedimentological interpretation and biomarker-derived absolute sea

136 surface temperature (SST) reconstructions from the same core (Hartman et al.,

137 submitted this volume) with our dinocyst assemblage data, we assess the

138 oceanographic variability off Wilkes Land from the dinocyst assemblages both at

139 glacial-interglacial and long-term times scales.

140

141   **2. Material**

142   2.1 Site description for IODP Hole U1356A

143   Samples were taken from IODP Hole U1356A, drilled on the continental rise of

144   the Wilkes Land Margin, East Antarctica (Figure 1a; present coordinates 63°18.6' S,

145   135°59.9' E; Escutia et al., 2011b). We use the paleolatitude calculator

146   www.paleolatitude.org of van Hinsbergen et al. (2015) to reconstruct the

147   paleolatitudinal history of the site (Figure 1, between -59.8±4.8°S and -61.5±3.3° S

148   between 34 Ma and 13 Ma, respectively). The single hole at Site U1356 reaches a

149   depth of 1006.4 m into the seabed (Escutia et al., 2011b). Oligocene to late Miocene

150   sediments were recovered between 890 and 3 mbsf (Figure 2; Tauxe et al., 2012;

151   revised according to Bijl et al., in press). The uppermost 95 meters of the hole were

152   poorly recovered; sediments consisted of unconsolidated mud strongly disturbed by

153   rotary drilling (Escutia et al., 2011b). Hence, we focused our investigation on the

154   interval between Cores 11R to 95R Section 3 (95.4 to 894 mbsf; 10.8-33.6 Ma; Figure

155   2).

156

157   2.2 Lithology in IODP Hole U1356A

158   In the studied interval between 95.4 and 894 mbsf, nine lithologic units have

159   been recognized during shipboard analysis (Figure 2; et al., 2011b). Salabarnada et al.

160   (submitted this volume) presents a detailed lithologic study of the Oligocene

161   sediments. For the grouping of our results, we use the lithologic facies from

162   Salabarnada et al. (submitted this volume), as outlined in Table 2. For the Miocene

163   interval of Site U1356, such a detailed lithologic description is not yet available;

164   therefore we treat the Miocene sediments as one separate lithologic unit in this

165   paper. For the Miocene, we here give a brief summary of the observations published

166   in the IODP Expedition 318 post-cruise report (Escutia et al., 2011b). Miocene

167   sediments between 95 and 400 mbsf reflect increasing consolidation down-core, and

168   comprise diatom ooze and diatom-rich silty clays. The more consolidated bedding has

169   caused better preservation of original bedding structures. From 278.4 to 459.4 mbsf,

170   the lithology lacks gravel-sized clasts, but is otherwise similar to up-core.

171

172   2.3 Bio-magnetostratigraphic age model for IODP Hole U1356A

173   Stratigraphic constraints for the Oligocene–Miocene succession from IODP

174   Hole U1356A are provided through calcareous nannoplankton, radiolarian, diatom

175   and sparse palynological biostratigraphy, complemented with magnetostratigraphy

176   (Tauxe et al., 2012). Bijl et al. (in press) and Crampton et al. (2016) have updated the

177   existing age model for Site U1356 for the Oligocene and Miocene part of the

178   succession, respectively. Thereby, they recalibrated to the international time scale of

179   Gradstein et al., 2012. We here follow these new insights of the age model (Table 1).

180   We infer ages by linear interpolation between tie points (Figure 2; Table 1).

181

182   2.4 Depositional setting IODP Site U1356

183   The depositional setting of Site U1356 changed from a shallow mid-

184   continental shelf in the early Eocene (Bijl et al., 2013a) to a deep continental rise

185   setting in the Oligocene (Houben et al., 2013) due to subsidence of the Wilkes Land

186   Margin (e.g., Close et al., 2009). Regional extrapolation of the lithology at U1356A via

187   seismic profiles suggests a mix of distal-fan and hemipelagic sedimentation during

188   the early Oligocene, grading into channel-levee deposits towards the later Oligocene

189   (Escutia et al., 2011b). The boundary between these two different depositional

190   settings occurs at ~650 mbsf; there, sedimentation rates increase, and the

191   documentation of mass-transport deposits from this depth upwards suggest shelf-

192   derived erosion events on the Wilkes Land continental slope (Escutia et al., 2011b).

193

194   **3. Methods**

195   3.1 Palynological sample processing

196   We refer to Bijl et al. (in press) for sample processing and analytical

197   procedures used. Both were according to standard procedures (e.g., Bijl et al., 2013b).

198   The 25 species of dinocysts new to science, which are formally (2 species) and

199   informally (23 species) described in Bijl et al. (in press) fit into known and extant

200   genera and therefore could be confidently included in the ecological groups as

201   described below.

202

203   3.2 Ecological grouping of dinocyst taxa

204   Bijl et al. (in press) provided additional statistical evidence to distinguish *in*

205   *situ* dinocysts from those that are reworked from older strata. In this paper, we follow

206   the interpretations of Bijl et al. (in press) and divide the dinocyst species into a

207   reworked and an *in situ* part (Table 3). To use the *in situ* dinocyst assemblages for

208   oceanographic reconstructions, we rely on the observation that many taxa in the

209   fossil assemblages have morphologically closely related modern counterparts. This

210   approach takes advantage of studies on present-day relationships between Southern

211   Ocean microplankton in general and dinoflagellates in particular and their surface-

212   water characteristics (e.g., Eynaud et al., 1999; Esper and Zonneveld, 2002, 2007;

213   Prebble et al., 2013). We assign Oligocene–Miocene dinocyst taxa to present-day eco-

214   groups interpreted from the clusters identified by Prebble et al. (2013), which seem

215   to be closely related to the oceanic frontal systems in the Southern Ocean (Figure 3).

216   Supporting evidence for the ecologic affinities for the dinocyst groups comes from

217   empirical data (Sluijs et al., 2005), for instance when it comes to the oceanic affinities

218   of *Nematosphaeropsis labyrinthus*, *Operculodinium* spp., *Pyxidinopsis* spp. and

219   *Impagidinium* spp. There is further abundant evidence, both empirically (e.g., Sluijs et

220   al., 2003; Houben et al., 2013) and from modern observations (Zonneveld et al., 2013;

221   Prebble et al., 2013; Eynaud et al., 1999), which link the abundance of

222   protoperidinioid dinocysts to high surface-water primary productivity. The arguably

223   most important inference from the surface-sample study of Prebble et al. (2013) is

224   that *Selenopemphix antarctica* is common to dominant (10-90%) in proximal sea-ice

225   settings south of the Antarctic polar front (AAPF). Notably, none of the surface

226   samples outside of the AAPF have dominant *Selenopemphix antarctica* (Prebble et al.,

227   2013). Another important observation is that the surface samples south of the AAPF

228   are devoid of gonyaulacean dinocysts, with the exception of two species of

229   *Impagidinium* (i.e., *I. pallidum* and *I. sphaericum*) which can occur, although neither

230   abundantly (Prebble et al., 2013) nor exclusively (e.g., Zevenboom, 1995; Zonneveld

231   et al., 2013), in ice-proximal locations. Another important observation is the

232   occurrence of abundant *Nematosphaeropsis labyrinthus* exclusively in regions outside

233   of the Subantarctic Front, and particularly close to the Subtropical Front. In summary,

234   from proximal Antarctic to outside the frontal systems, Prebble et al. (2013)

235   documents dominance of *S. antarctica* south of the AAPF, dominance of other

236   protoperidinioid dinocysts at and N of the AAPF, mixed protoperidinioid and

237   gonyaulacoid dinocysts (with a notable common occurrence of *Nematosphaeropsis*

238   *labyrinthus* at the SAF and mixed gonyaulacoid dinocysts at and outside of the STF.

239   These trends represents the transition from sea-ice influenced to cold upwelling/high

240   nutrient to warm-temperate/lower nutrient conditions, respectively. We use the

241   affinities obtained by Prebble et al. (2013) to reconstruct past oceanographic

242   conditions at the Wilkes Land continental margin.

243

244   **4. Results**

245   4.1 Palynological groups

246   In our palynological analysis we separated palynomorph groups into four

247   categories: *In situ* dinocysts, reworked dinocysts (following Bijl et al. (in press); Table

248   3), acritarchs and terrestrial palynomorphs. Our palynological slides further contain a

249   varying amount of pyritized diatoms and a minor component of amorphous

250   palynofacies, which is not further considered in this study. The relative abundance of

251   the four palynomorph groups varies considerably throughout the record, as do their

252   absolute abundances (Figure 4). Reworked dinocysts are present to common

253   throughout the record, but are particularly abundant in the lowermost 40 meters of

254   the Oligocene and in the Upper Oligocene. *In situ* dinocysts dominate the

255   palynomorph assemblage during the mid-Oligocene and mid-Miocene. Chorate,

256   spheromorph and *Cymatiosphaera*-type acritarchs (which are not further

257   taxonomically subdivided in this study) dominate the assemblage during the late

258   Oligocene and into the mid-Miocene, while terrestrial palynomorphs (which are

259   considered *in situ* and not reworked from older strata (Strother et al., 2017)) are a

260   constant minor component of the total palynomorph assemblage (Fig. 4).

261

262   4.2 *In situ* dinocyst assemblages

263   Throughout the Oligocene, *in situ* dinocyst assemblages are dominated by

264 protoperidinioid dinocysts, notably *Brigantedinium* spp., *Lejeunecysta* spp., *Malvinia*

265 *escutiana,* and *Selenopemphix* spp. (Figure 4)*,* all of which are considered associated

266 with heterotrophic dinoflagellates. Among these protoperidinioid cysts, *S. antarctica*

267 is common to abundant only in the first 1.5 million years of the Oligocene

268 represented in the core material (33.6–32.1 Ma), and during and after the mid-

269 Miocene climatic transition (<14.2 Ma; Fig. 5). The remainder of the record is

270 generally devoid of *S. antarctica*. This is much in contrast to the dinocyst assemblages

271 at Site U1356 today, which are dominated by this taxon (Prebble et al., 2013). Instead,

272 other protoperidinioid dinocysts dominate, such as *Brigantedinium* spp., several

273 *Lejeunecysta* species and *Selenopemphix nephroides*, which have close affinities to

274 high-nutrient conditions in general (e.g., Harland et al., 1999; Zonneveld et al., 2013)

275 but are not specifically restricted to sea-ice-proximity or the Southern Ocean. Today,

276 these three genera dominate dinocyst assemblages in high-nutrient regions at or

277 outside of the AAPF (Prebble et al., 2013). We also encountered a varying abundance

278 of protoperidinioid dinocysts, which could not be placed with confidence into

279 established protoperidinioid dinocyst genera. These are grouped under

280 protoperidinioid spp. pars (Figure 4), and are here assumed to exhibit the same

281 heterotrophic life-style as the other protoperidinioid dinocyst genera.

282 Next to peridinioid dinocysts, also gonyaulacoid dinocysts occur commonly to

283 abundantly throughout the record from Site U1356. They comprise both known and

284 previously unknown (Bijl et al., in press) species of *Batiacashaera, Pyxidinopsis,*

285   *Nematosphaeropsis, Impagidinium,* and *Operculodinium* (Fig. 4; 5). Except for the

286   extinct genus *Batiacasphaera*, all the other genera are still extant and are formed by

287   phototrophic dinoflagellates. The abundance of these presumably mostly autotrophic

288   taxa (Zonneveld et al., 2013) goes at the expense of the assumed heterotrophic

289   protoperidinioid dinocysts. A remarkable increase is noted associated with the mid-

290   Miocene Climate Optimum (between ~17 and 15 Ma; Fig. 4, 5; Sangiorgi et al., in

291   review). Of these taxa, *Nematosphaeropsis* is thought to be associated with frontal

292   systems of the present-day Southern Ocean (Prebble et al., 2013) and also in the

293   North Atlantic Ocean (Boessenkool et al., 2001; Zonneveld et al., 2013).

294

295   4.5 Comparison between palynological data and lithological interpretations

296   The Oligocene sediments from Site U1356 comprise distinctive alternations of

297   lithologic facies throughout the section (Salabarnada et al., submitted this volume;

298   Figure 2). They are interpreted to reflect changes in the oceanographic regime, with

299   relations to glacial-interglacial changes (Salabarnada et al., submitted this volume).

300   Carbonate deposits, pelagic claystones and bioturbated, carbonate-bearing silty

301   claystones were interpreted as interglacial deposits, while the laminated lithologies

302   reflect glacial deposits (Salabarnada et al., submitted this volume). Mass-transport

303   deposits reflect times of major sediment transport from the continental shelf. The

304   lower Oligocene glauconitic sandstones were interpreted to reflect episodes of

305   redeposition of winnowed upper Eocene shelf sediments (Sluijs et al., 2003; Houben,

306   2012). We here evaluate and compare the palynological content of each of these

307   lithologies, both in terms of absolute and relative abundance of the main

308   palynomorph groups: reworked dinocysts, *in situ* dinocysts, acritarchs and terrestrial

309   palynomorphs and relative abundance of *in situ* dinocyst eco-groups.

310

311   4.5.1 Palynomorph groups and lithology

312   There are distinct differences in the relative and absolute abundances of

313   palynomorph groups between the different lithologies (Figure 6). The highest relative

314   and absolute abundances of reworked dinocysts occur in the lower Oligocene

315   reworked glauconitic sandstones, which is in line with previous inferences of Houben

316   et al. (2013). The mass-transport deposits contain abundant reworked dinocysts. The

317   relative and absolute abundance of *in-situ* dinocysts does not vary much between the

318   different lithologies, with the exception of the pelagic clays, in which *in situ* dinocysts

319   are much lower in relative and absolute abundance (Figure 6). The opposite pattern

320   emerges for acritarchs, which reach highest relative and absolute abundances in the

321   pelagic clays (Figure 6). Terrestrial palynomorphs are most abundant in the

322   glauconitic contorted sandstones (Figure 6).

323

324   4.5.2 *In situ* dinocyst eco-groups and lithology

325   We also compared the *in situ* dinocyst eco-groups with predominant

326   lithological facies (Figure 7). The abundance of *Selenopemphix antarctica* is low

327   throughout the record (0-5%), with the exception of the interval post-dating the

328   Miocene Climatic Optimum (MCO) interval and the lowermost Oligocene. We note

329   that in the lower Oligocene, high abundances of *S. antarctica* and *Malvinia escutiana*

330   are mostly connected to glauconitic sandstones and the mass-transport deposits, and

331   rarely occur in the other lithologies (Figure 7). We however think that these species

Climate
of the Past
Discussions

332   represent part of the *in situ* assemblage in an otherwise dominantly reworked

333   dinocyst assemblage, because these were never found in Eocene sediment in the

334   region before. *Lejeunecysta* spp. shows significantly higher relative abundances in the

335   mass-transport and glacial deposits, and substantially lower abundance in the pelagic

336   clays, interglacial deposits and in the Miocene. *Brigantedinium* spp. shows invariable

337   relative abundances in the different lithologies, and the *Protoperidinium* spp. pars

338   group shows highest abundance in the pelagic clays (Figure 7). Overall, the relative

339   abundances of all (proto)peridinioid dinocysts in the *in situ* assemblage is highest in

340   the glacial deposits and pelagic clays, and substantially lower in interglacial deposits

341   and in the Miocene. Indeed, several gonyaulacoid dinocyst taxa (such as

342   *Nematosphaeropsis* spp., *Pyxidinopsis* cpx, *Operculodinium* spp., and *Impagidinium*

343   spp.) show higher relative abundances in interglacial than in glacial deposits. We thus

344   observe a marked difference in the relative abundances of gonyaulacoid dinocysts

345   over peridinioid dinocysts between glacial and interglacial deposits.

346

347   **5. Discussion**

348   5.1 Paleoceanographic interpretation of the dinocyst assemblages

349   5.1.1 Surface-ocean nutrient conditions

350   The dominance of heterotrophic dinoflagellate cysts in the Oligocene-Miocene

351   dinocyst assemblages indicate overall high nutrient levels in the surface waters. We

352   infer therefore that in general, surface-waters overlying Site U1356 experienced

353   upwelling associated to the AAPF during most of the Oligocene and Miocene.

354   However, and surprisingly, the occasionally abundant oligotrophic cyst taxa

355   encountered in our record suggest that at times, surface waters were much less

Climate
of the Past
Discussions

356   nutrient-rich, supporting an oligotrophic dinoflagellate assemblage. These dinocysts

357   are outer shelf to oceanic or outer neritic taxa (e.g., Sluijs et al., 2005; Zonneveld et al.,

358   2013; Prebble et al., 2013), which makes it unlikely they were reworked from the

359   continental shelf. Indeed, these taxa show low relative abundances in the mass-

360   transport deposits (Figure 6); hence, we interpret that these taxa are part of the *in

361   situ* pelagic assemblage and reflect warming of surface waters rather than them being

362   reworked. Although species within these genera have relatively long stratigraphic

363   ranges extending back into the Eocene, most of the species encountered at U1356

364   have never been found in Eocene continental shelf sediments in the region (e.g., Bijl et

365   al., 2011; 2013a, b; Brinkhuis et al., 2003a, b; Levy and Harwood, 2000; Wrenn and

366   Hart, 1988). This lends further support against them being reworked from Eocene

367   shelf material, in addition, the statistical approach also interprets these species to be

368   part of the *in situ* assemblage (Bijl et al., in press). Now that we have abundant

369   evidence that these autotrophic taxa are part of the *in situ* pelagic assemblage, we can

370   interpret these assemblages in terms of their paleoceanographic affinities. The

371   occasional abundance of oligotrophic taxa suggests nutrient levels must have been

372   low compared to the same region today. The absence of these taxa in modern surface

373   waters south of the AAPF is probably caused by a combination of factors: low sea

374   surface temperatures, isolation by strong eastward currents, but also the abundance

375   and seasonal concentration of nutrients, which make the Antarctic proximal surface

376   waters a very specialistic niche. Apparently, surface water conditions during the

377   Oligocene and Miocene were such that these oligotrophic species could at times

378   proliferate so close to the Antarctic margin.

379

380   5.1.2 sea-surface temperature

381   The average dinocyst assemblages in our record point to the Southern margin of New

382   Zealand and Tasmania as the best modern analogue (inferred from Prebble et al.,

383   2013; Figure 2). Those regions today feature a mix between protoperidinioid

384   dinocysts and gonyaulacoid dinocyst genera such as *Nematosphaeropsis*,

385   *Operculodinium* and *Impagidinium*. These assemblages occur at present in surface-

386   waters with mean annual temperatures of 8-17°C (Prebble et al., 2013). A bayesian

387   approach on the TEX_{86} index values at U1356 (presented in Sangiorgi et al.,

388   submitted; Hartman et al., submitted this volume) indicates exactly the same region

389   as modern analogues for the TEX_{86} index values found (Hartman et al., submitted this

390   volume) as for the dinocysts (Prebble et al., 2013); both approaches indicate the same

391   paleotemperature range for the Oligocene-Miocene at U1356. These two proxies thus

392   independently point to a temperate, much warmer paleoceanographic regime close to

393   Antarctica during the Oligocene and Miocene with the nearest modern analogue

394   being offshore Southern New Zealand and Tasmania. Supporting evidence for

395   temperate Oligocene-Miocene surface waters comes from the abundance of

396   nannofossils encountered in the same Oligocene-Miocene sediments (Escutia et al.,

397   2011b). Today, carbonate-producing plankton is not abundant in high-latitude

398   surface waters south of the AAPF (Eynaud et al., 1999). Moreover, the remains of the

399   few carbonate-producing organisms living at high latitudes rarely reach the ocean

400   floor because strong upwelling of relatively CO_2-rich, corrosive waters (e.g., Olbers et

401   al., 2004). Hence, the presence of carbonate-rich intervals during the Oligocene-

402   Miocene at Site U1356, along with the encountered oligotrophic, temperate dinocysts,

403   suggests fundamentally warmer surface-water conditions than at present.

Climate
of the Past
Discussions

404

405   5.1.3 Paleoceanography

406   The strong similarity of Oligocene–Miocene dinocyst assemblages at Site

407   U1356 to those today occurring much further north (e.g., around Tasmania and

408   Southern New Zealand (Prebble et al., 2013) suggests a fundamentally different

409   *modus operandi* of Southern Ocean oceanography. The strict latitudinal separation of

410   dinocyst assemblages throughout the Southern Ocean today (Prebble et al., 2013) is

411   likely due to the different water masses present across the oceanic fronts where

412   strong wind-driven divergence around 60° S (known as the Antarctic Divergence; e.g.,

413   Olbers et al., 2004), strong sea-ice season and/or the vigorous Antarctic Circumpolar

414   Current are in place. The strength and position of the AAPF during the Oligocene–

415   Miocene is not well understood. GCM experiments under Miocene boundary

416   conditions suggest that west and east wind drifts prevailed south and north of 60°S,

417   respectively (Herold et al., 2011). This position of the winds determines the average

418   position of the Antarctic Divergence at 60°S during the Oligocene and Miocene, like

419   today. This would mean that Site U1356 likely was directly overlain by the AAPF.

420   However, the significantly warmer, more oligotrophic character of the dinocyst

421   assemblages offshore Wilkes Land throughout the Oligocene–Miocene argues against

422   a close position to the AAPF. The position of the AAPF relative to the position of Site

423   U1356 strongly determines the likelihood of southward transport of low-latitude

424   waters towards the site. A southward position of the AAPF relative to Site U1356

425   would greatly enhance the possibility for southward migration of temperate water

426   masses towards the site. A northward position of the AAPF relative to the site, would

427   make such much more difficult. The presence of carbonate in these deep marine

18

Climate
of the Past
Discussions

Open Access

EGU

428   sediments also suggests that upwelling of corrosive waters through the (proto-)

429   Antarctic Divergence was either much reduced or located elsewhere. Therefore, we

430   deduce that the occurrence of the oligotrophic, temperate dinocysts is evidence for a

431   southward position of the AAPF relative to the position of Site U1356.

432   The separate averaging of dinocyst assemblages for glacial and interglacial

433   deposits (Figure 7) allows us to reconstruct the glacial-interglacial surface

434   oceanographic changes throughout the Oligocene. This approach suggests that

435   substantial paleoceanographic dynamics were associated with Oligocene glacial-

436   interglacial cycles. Alongside the 2–3 °C SST variability during glacial-interglacial

437   cycles at this same site (Hartman et al., submitted this volume), dinocyst assemblages

438   contain more oligotrophic, temperate dinocysts during interglacial time intervals

439   compared to glacial intervals when more eutrophic, colder dinocysts proliferated.

440   This could be the result of a slight latitudinal movement of oceanic frontal systems

441   (notably the AAPF), as has been reconstructed for the Southern Ocean fronts during

442   the most recent glacial to interglacial transition (e.g., Kohfeld, et al. 2013). The

443   difference in dinocyst assemblages between glacial and interglacial deposits might be

444   explained by a south position of the AAPF during interglacials, allowing for temperate

445   oligotrophic surface waters to reach the Site, while during glacials the AAPF migrated

446   northward over Site U1356, causing cold, high-nutrient conditions.

447

448   5.2 Implications for Oligocene-Miocene ocean circulation

449   Only in the lowermost Oligocene and in strata representing the mid-Miocene

450   climatic transition and later (14.4 Ma and younger), the dinocyst assemblages bear

451   similarities to modern proximal-Antarctic assemblages (Prebble et al., 2013), with

Climate
of the Past
Discussions

452   high abundances of *Selenopemphix antarctica*. Even in those intervals, however, the

453   relative abundances of *S. antarctica* does not reach present-day values at the same

454   site. The absence of a strong shift towards modern-day-like assemblages in our

455   record can be interpreted to reflect a weaker-than-present ACC, in line with

456   numerical models (Herold et al., 2012; Hill et al., 2013). The ACC itself represents an

457   important barrier for latitudinal surface-water transport towards the Antarctic

458   margin, in addition to the Antarctic Divergence (Olbers et al., 2004). Our data suggest

459   an increase in the influence of oligotrophic dinocysts at the Antarctic margin during

460   the late Oligocene and during the MMCO, which argues against the installation of a

461   vigorous ACC at 30 Ma (Scher et al., 2015): No profound changes in surface

462   paleoceanography emerge from our dinoflagellate cyst data around 30 Ma, and there

463   is no major change in the benthic $\delta^{18}O$ (Figure 5). Instead, if the Tasmanian Gateway

464   had opened to an extent that allowed ACC development (Scher et al., 2015), the ACC

465   must have been much weaker than at present throughout the Oligocene and Miocene.

466   The strongly different dinocyst assemblages compared to present-day at Site U1356

467   throughout our record implies to us that a strong coherent ACC was not installed until

468   after the MMCT (11 Ma). This is consistent with inferences from the lithology at the

469   same site (Salabarnada et al., submitted this volume), suggesting a proto-ACC much

470   weaker than at present and, likewise, weaker Southern Ocean frontal systems. An

471   alternative explanation is that the ACC increased in strength during the Oligocene–

472   Miocene, but that this strengthening had no influence on the dinocyst assemblages at

473   Site U1356. However, the vigorous nature of the ACC influencing surface as well as

474   bottom waters and governing eddy water circulation in the Southern Ocean (Olbers et

475   al., 2004) makes such a scenario very unlikely. Nevertheless, to firmly clarify whether

476 the strength of the ACC changed to its present-day force only after the MMCT (as

477 suggested by our data), ocean-circulation modelling of time slices younger than the

478 Oligocene will be required.

479

480   5.3 Implications for ice sheet and sea-ice variability

481   The abundance of our sea-ice indicator *Selenopemphix antarctica* throughout

482 the record is consistently lower than that in present-day dinocyst assemblages at Site

483 U1356 (Prebble et al., 2013; Figure 3). This suggests that sea-ice conditions were

484 never as severe as today throughout the studied time interval. Only during two time

485 intervals sea ice indicators suggest some sea ice near the Site: the first 1.5 million

486 years following the Oi-1 glaciation (33.6–32.1 Ma; Figure 5), and during and after the

487 mid-Miocene climatic Transition (14–11 Ma; Figure 5). Numerical ice-sheet/sea-ice

488 modelling (DeConto et al., 2007) suggests sea-ice to develop only if the continental ice

489 sheets reach the coastline. Our lack of sea-ice indicators during most of the Oligocene

490 and Miocene could thus suggest that the Antarctic continental ice sheet was much

491 reduced during this time. The finding of a weaker sea-ice season throughout most of

492 the Oligocene–Miocene at Site U1356 has major implications for regional

493 paleoceanography because it suggests a decrease in the potential formation of

494 Antarctic bottom waters at this site.

495   The abundance of our oligotrophic taxa broadly co-varied with long-term

496 Oligocene-Miocene benthic $\delta^{18}O$: During times of low $\delta^{18}O$ values in deep-sea benthic

497 foraminifera (and thus high deep-sea temperatures and less ice volume; e.g., at 32 Ma,

498 24 Ma and 15 Ma; Figure 5), the abundance of oligotrophic temperate dinocysts was

499 large (Figure 5). At times of higher $\delta^{18}O$ values, lower deep-sea temperatures and

21

500 higher ice volume (e.g. at 33.5 Ma, 27 Ma, 23 Ma and 13 Ma; Figure 5) temperate

501 dinocysts were reduced in abundance and high-nutrient, sea-ice indicators

502 (re)appeared. Altogether, this suggests on long time scales, that there was stronger

503 influence of warm surface waters at the Wilkes Land Margin at times when ice sheets

504 were smaller and climate was warmer, and less influence of warm surface waters

505 during times of larger ice sheets, hence a connection between ice sheet and

506 oceanographic variability.

507   Oxygen-isotope mass-balance calculations suggest that a modern-day-sized

508 Antarctic ice sheet appeared at the Eocene/Oligocene boundary (DeConto et al.,

509 2008). Benthic $\delta^{18}O$ records suggest that ice sheets fluctuated considerably in size

510 during the subsequent Oligocene and Miocene (Liebrand et al., 2017). Based on the

511 heavy $\delta^{18}O$ values for Oligocene benthic foraminifera from Maud Rise, it was inferred

512 that Antarctic ice sheets were near-present-day size throughout the Oligocene

513 (Hauptvogel et al., 2017). Both isotope studies of Liebrand et al (2017) and

514 Hauptvogel et al. (2017) assume constant temperatures of the deep sea and similar-

515 to-present-day $\delta^{18}O$ of the continental ice. Our data instead show that the regional

516 paleoceanography, together with surface-ocean temperature (Hartman et al.,

517 submitted this volume), can vary considerably both on the long term as on orbital

518 time scales. It remains to be seen whether the variability in paleoceanography found

519 here can be extrapolated to larger parts of the Antarctic margin, including to those

520 regions of deep-water formation. Given the high temperatures and absence of strong

521 sea ice influence, the Wilkes Land margin was likely not the primary sector of deep-

522 water formation, although there is ample evidence for bottom-current activity at the

523 site (Salabarnada et al., submitted this volume). However, if the oceanographic and

524   climate variability we reconstruct offshore Wilkes Land characterises also regions of

525   deep-water formation, some (if not much) of the variability both on long and on

526   orbital time scales in benthic δ^{18}O records is related to deep-sea temperature rather

527   than Antarctic ice volume (see also Hartman et al., submitted this volume).

528   Meanwhile, we find little support in our study for the large continental ice sheets

529   during the Oligocene as concluded by Hauptvogel et al. (2017), given the absence of

530   dominance of sea-ice dinoflagellate cysts and *in situ* terrestrial palynomorphs

531   (Strother et al., 2017). As an alternative explanation to the difference in δ^{18}O values

532   between Maud Rise and Equatorial Pacific during the Oligocene (Hauptvogel et al.,

533   2017), we suggest that these two records have recorded the characteristics of two

534   fundamentally different deep water masses, with those at Maud Rise being much

535   colder and saltier than those at Shatsky Rise.

536

537   **6. Conclusions**

538   The dinocyst assemblage changes in the Oligocene–Miocene (33.6–10 Ma) of Site

539   U1356 were interpreted in terms of surface paleoceanography based on a

540   comparison of these assemblages to present-day dinocyst assemblages. This

541   approach allows us to hypothesize that the Southern Ocean paleoceanography during

542   the Oligocene–Miocene was fundamentally different from that of today. A strong sea-

543   ice signal (yet still weaker than that of today) emerges for the Wilkes Land Margin

544   only for the first 1.5 million years of the Oligocene (33.6–32.1 Ma) and the mid-

545   Miocene climatic transition (14-10 Ma). The remainder of the Oligocene–Miocene

546   record of surface waters off Wilkes Land were warm, relatively oligotrophic and lack

547   indications of a prominent sea-ice season. Upwelling at the Antarctic Divergence must

548   have been profoundly weaker during Oligocene and Miocene times, compared to

549   today. Furthermore, the continental ice sheet must have been much reduced at the

550   Wilkes Land sub-glacial basin for most of the Oligocene-Miocene compared to today,

551   and continental ice sheets were retreated inland. The strength of the influence of

552   warm oligotrophic surface water was strongly coupled to deep-sea $\delta^{18}O$ values: With

553   enhanced low-latitude influence of surface water during times of light $\delta^{18}O$ in the

554   deep sea and *vice versa*. The absence of (a trend towards more) oceanographic

555   isolation of the Wilkes Land margin throughout the Oligocene to mid-Miocene

556   suggests that the ACC did not obtain its full, present-day strength until at least the

557   mid-Miocene Climatic transition. Moreover, we note considerable glacial-interglacial

558   variability in this oceanographic setting, with stronger influence of oligotrophic, low-

559   latitude surface waters over Site U1356 during interglacial times and more eutrophic,

560   colder influence during glacial times. This may suggest considerable latitudinal

561   migration of the AAPF over Oligocene and Miocene glacial-interglacial cycles.

562

563   **Acknowledgements**

571

Climate
of the Past
Discussions

Open Access

EGU

Author contributions

572

573   PKB, FS, CE and JP designed the research. AJPH, FS and PKB carried out dinoflagellate

574   cyst analyses for the earliest Oligocene, the middle Miocene, and the Oligocene-

575   Miocene boundary interval, respectively. AS and CE provided the lithological data.

576   PKB integrated, cross-validated and compiled the data, and wrote the paper with

577   input from all co-authors.

578

579

Climate
of the Past
Discussions

Open Access

EGU

580 **Figure captions**

581 Figure 1 Paleogeography of the Southwest Pacific Ocean and position of IODP Site

582 U1356 (Red star) at (a) 0 Ma, (b) 10 Ma, (c) 20 Ma, and (d) 30 Ma. Figures were

583 modified from Bijl et al. (in press). Reconstructions were adapted from G-plates, with

584 plate circuit from Seton et al. (2012) and absolute plate positions of Torsvik et al.

585 (2012).

586

587 Figure 2. Age model for the Oligocene–Miocene interval of Hole U1356A. Core

588 recovery, lithostratigraphic units and log, age-depth plot (from Tauxe et al., 2012, but

589 recalibrated to GTS2012 of Gradstein et al., 2012; see Table 1 and modified based on

590 Crampton et al., 2016), and samples taken for palynology. Figure modified from Bijl et

591 al. (in press).

592

593 Figure 3. Generic representation of present-day distributions of dinocysts in surface

594 sediments in the Southern Ocean. The dinocyst pie charts represent average

595 dinoflagellate cyst assemblage compositions for surface sediments underneath

596 oceanic frontal zones in the Southern Ocean. Figure modified from Sangiorgi et al. (in

597 review), data replotted from Prebble et al. (2013).

598

599 Figure 4. Core recovery, lithostratigraphic log (after Salabarnada et al., this volume),

600 chronostratigraphic epochs (E = Eocene) and stages (L = Lutetian, Burd. =

601 Burdigalian, Ser. = Serravallian, T. = Tortonian), absolute palynomorph (grey) and *in*

602 *situ* dinocyst (black) concentrations (# per gram of dry sediment, presented on a

603 logarithmic scale), palynomorph content (reworked dinocysts, *in situ* dinocysts,

604   acritarchs, and terrestrial palynomorphs; given in percentages of total

605   palynomorphs), and relative abundance of *in situ* dinocyst assemblages (in

606   percentage of *in situ* dinocysts) for the Oligocene–Miocene of Hole U1356A.

607

608   Figure 5. Benthic foraminiferal oxygen isotope data from Site 588 (Zachos et al.,

609   2008), Site 1090 (Zachos et al., 2008) Site 1218 (recalibrated from (Pälike et al.,

610   2006), Site U1334 (Holbourn et al., 2015), Site U1337 (Beddow et al., 2016), with

611   Dinocyst assemblage data from Site U1356. We used the paleomagnetic tie points of

612   Tauxe et al. (2012) (with the exception of the Oligocene–Miocene boundary interval,

613   see text) recalibrated to Gradstein et al. (2012) for calibrating our data to age,

614   following the age-depth model specified in Figure 2 and Table 1.

615

616   Figure 6. Comparison of relative (left bar; in % of total palynomorphs) and absolute

617   (right bar, in $\# * gr^{-1}$ dry weight) abundances of palynomorph groups per lithology.

618   Average (black lines) and standard deviation (coloured bars) of absolute and relative

619   abundances of total palynomorphs, reworked dinocysts, *in situ* dinocysts, acritarchs

620   and terrestrial palynomorphs grouped in the different lithologies: Miocene

621   sediments, carbonate deposits, bioturbated sediments, pelagic clays, laminated silty

622   claystones, laminated sand stones, mass-transport deposits and glauconitic sand

623   stones.

624

625   Figure 7. Comparison of *in situ* eco-groups with lithology. Average (black line) and

626   standard deviation (coulored bar) of relative abundances of grouped taxa from

627   samples from the different lithologies: Miocene sediments, carbonate deposits,

628   bioturbated sediments, pelagic clays, laminated silty claystones, laminated sand

629   stones, mass-transport deposits and glauconitic sand stones.

630

631   **Table captions**

632   Table 1. Age constraints for the Oligocene–Miocene of Hole U1356A.

633   Table 2. Lithologic facies described in Salabarnada et al. (submitted this volume), and

634   in this paper.

635   Table 3. List of assumed *in situ* and reworked dinoflagellate cyst taxa encountered in

636   this study. See Bijl et al. (in press) for informal species descriptions, and discussion

637   about which species are considered reworked and *in situ*.

638

Climate
of the Past

Discussions

639   References

640 Badger, M.P.S., Lear, C.H., Pancost, R.D., Foster, G.L., Bailey, T.R., Leng, M.J., Abels, H.A.,
641 2013. CO_2 drawdown following the middle Miocene expansion of the Antarctic Ice Sheet.
642 Paleoceanography 28, 42-53.

643 Barker, P., Camerlenghi, A., Acton, G., Brachfeld, S., Cowan, E., Daniels, J., Domack, E., Escutia,
644 C., Evans, A., Eyles, N., Guyodo, Y., Iorio, M., Iwai, M., Kyte, F., Lauer, C., Maldonado, A.,
645 Moerz, T., Osterman, L., Pudsey, C., Schuffert, J., Sjunneskog, C., Vigar, K., Weinheimer, A.,
646 Williams, T., Winter, D., Wolf-Welling, T., 1998. Antarctic glacial history and sea-level change -
647 Leg 178 samples Antarctic Peninsula margin sediments. JOIDES Journal 24, 7-10.

648 Barker, P.F., Barrett, P.J., Cooper, A.K., Huybrechts, P., 1999. Antarctic glacial history from
649 numerical models and continental margin sediments. Palaeogeography, Palaeoclimatology,
650 Palaeoecology 150, 247-267.

651 Barker, P.F. and Thomas, E., 2004. Origin, signature and paleoclimatic influence of the Antarctic
652 Circumpolar Current. Earth Science Reviews 66, 143-162.

653 Barrett, P.J., 1989. Antarctic Cenozoic history from the CIROS-1 drillhole, McMurdo Sound.
654 Science Information Publishing Centre DSIR Bulletin, volume 245, Wellington.

655 Beddow, H.M., Liebrand, D., Sluijs, A., Wade, B.S., Lourens, L.J., 2016. Global change across the
656 Oligocene-Miocene transition: High-resolution stable isotope records from IODP Site U1334
657 (equatorial Pacific Ocean). Paleoceanography 31, 81-97.

658 Bijl, P.K., Bendle, A.P.J., Bohaty, S.M., Pross, J., Schouten, S., Tauxe, L., Stickley, C.E., McKay,
659 R.M., Röhl, U., Olney, M., Sluijs, A., Escutia, C., Brinkhuis, H., Expedition 318 scientists, 2013a.
660 Eocene cooling linked to early flow across the Tasmanian Gateway. Proceedings of the National
661 Academy of Sciences of the United States of America 110, 9645-9650.

662 Bijl, P.K., Houben, A.J.P., Schouten, S., Bohaty, S.M., Sluijs, A., Reichart, G.J., Sinninghe
663 Damsté, J.S., Brinkhuis, H., 2010. Transient Middle Eocene Atmospheric Carbon Dioxide and
664 Temperature Variations. Science 330, 819-821.

665 Bijl, P.K., Pross, J., Warnaar, J., Stickley, C.E., Huber, M., Guerstein, R., Houben, A.J.P., Sluijs,
666 A., Visscher, H., Brinkhuis, H., 2011. Environmental forcings of Paleogene Southern Ocean
667 dinoflagellate biogeography. Paleoceanography 26, PA1202.

668 Bijl, P.K., Sluijs, A., Brinkhuis, H., 2013b. A magneto- chemo- stratigraphically calibrated
669 dinoflagellate cyst zonation of the early Paleogene South Pacific Ocean. Earth-Science Reviews
670 124, 1-31.

671 Boessenkool, K.P., Van Gelder, M., Brinkhuis, H., Troelstra, S.R., 2001. Distribution of organic-
672 walled dinoflagellate cysts in surface sediments from transects
673 across the Polar Front offshore southeast Greenland. J. Quaternary Sci. 16, 661–666.

674 Brinkhuis, H., Munsterman, D.M., Sengers, S., Sluijs, A., Warnaar, J., Williams, G.L., 2003a. Late
675 Eocene to Quaternary dinoflagellate cysts from ODP Site 1168, off western Tasmania, in: Exon,
676 N., Kennett, J. P. (Eds.), Proceedings of the Ocean Drilling Program, Scientific Results, volume
677 189. U.S. Government Printing Office, College Station, Texas.

678 Brinkhuis, H., Sengers, S., Sluijs, A., Warnaar, J., Williams, G.L., 2003b. Latest Cretaceous to
679 earliest Oligocene, and Quaternary dinoflagellates from ODP Site 1172, East Tasman Plateau, in:
680 Exon, N., Kennett, J. P. (Eds.), Proceedings of the Ocean Drilling Program, Scientific Results,
681 volume 189. U.S. Government Printing Office, College Station, Texas.

Climate
of the Past
Discussions

682   Close, D.I., Watts, A.B., Stagg, H.M.J., 2009. A marine geophysical study of the Wilkes Land
683   rifted continental margin, Antarctica. Geophysical Journal International 177, 430-450.

684   Cook, C.P., Van De Flierdt, T., Williams, T., Hemming, S.R., Iwai, M., Kobayashi, M., Jimenez-
685   Espejo, F.J., Escutia, C., González, J.J., Khim, B., McKay, R.M., Passchier, S., Bohaty, S.M.,
686   Riesselman, C.R., Tauxe, L., Sugisaki, S., Galindo, A.L., Patterson, M. O., Sangiorgi, F., Pierce, E.
687   L., Brinkhuis, H., Klaus, A., Fehr, A., Bendle, J.A.P., Bijl, P.K., Carr, S.A., Dunbar, R.B., Flores,
688   J.A., Hayden, T.G., Katsuki, K., Kong, G.S., Nakai, M., Olney, M.P., Pekar, S.F., Pross, J., Röhl,
689   U., Sakai, T., Shrivastava, P.K., Stickley, C.E., Tuo, S., Welsh, K., Yamane, M., 2013. Dynamic
690   behaviour of the East Antarctic ice sheet during Pliocene warmth. Nature Geoscience 6, 765-769.

691   Cooper, A.K. and O'Brien, P.E., 2004. Leg 188 synthesis: Transitions in the glacial history of the
692   Prydz Bay region, East Antarctica, from ODP drilling. Proceedings of the Ocean Drilling Program:
693   Scientific Results 188, 1-42.

694   Crampton, J.S., Cody, R.D., Levy, R., Harwood, D., McKay, R., Naish, T.R., 2016. Southern
695   Ocean phytoplankton turnover in response to stepwise Antarctic cooling over the past 15 million
696   years. Proceedings of the National Academy of Sciences of the United States of America. 113,
697   6868-6873.

698   DeConto, R.M., Pollard, D., Harwood, D., 2007. Sea-ice feedback and Cenozoic evolution of
699   Antarctic climate and ice sheets. Paleoceanography 22, PA3214.

700   DeConto, R.M., Pollard, D., Wilson, P.A., Pälike, H., Lear, C.H., Pagani, M., 2008. Thresholds for
701   Cenozoic bipolar glaciation. Nature 455, 652-657.

702   Escutia, C., Brinkhuis, H., Klaus, A., 2011a. IODP expedition 318: From greenhouse to icehouse at
703   the Wilkes Land Antarctic margin. Scientific Drilling 15-23.

704   Escutia, C., Brinkhuis, H., Klaus, A., Party, Expedition 318 Scientists, 2011b. Proceedings of the
705   Integrated Ocean Drilling Program, Initial Results, volume 318. Tokyo (Integrated Ocean Drilling
706   Program Management International, Inc.).

707   Esper, O. and Zonneveld, K.A.F., 2007. The potential of organic-walled dinoflagellate cysts for the
708   reconstruction of past sea-surface conditions in the Southern Ocean. Marine Micropaleontology 65,
709   185-212.

710   Esper, O. and Zonneveld, K.A.F., 2002. Distribution of organic-walled dinoflagellate cysts in
711   surface sediments of the Southern Ocean (eastern Atlantic sector) between the Subtropical Front
712   and the Weddle Gyre. Marine Micropaleotology 46, 177-208.

713   Exon, N.F., Kennet, J.P., Malone, M., 2004. Leg 189 Synthesis: Cretaceous- Holocene history of
714   the Tasmanian Gateway. In Exon, N.F., Kennett, J.P., and Malone, M.J. (Eds.), Proceedings of the
715   Ocean Drilling Program, Scientific Results, Volume 189.

716   Eynaud, F., Giraudeau, J., Pichon, J., Pudsey, C.J., 1999. Sea-surface distribution of
717   coccolithophores, diatoms, silicoflagellates and dinoflagellates in the South Atlantic Ocean during
718   the late austral summer 1995. Deep-Sea Research Part I: Oceanographic Research Papers 46, 451-
719   482.

720   Foster, G.L., Lear, C.H., Rae, J.W.B., 2012. The evolution of pCO_2, ice volume and climate during
721   the middle Miocene. Earth and Planetary Science Letters 341-344, 243-254.

722   Foster, G.L. and Rohling, E.J., 2013. Relationship between sea level and climate forcing by CO_2 on
723   geological timescales. Proceedings of the National Academy of Sciences of the United States of
724   America 110, 1209-1214.

725 Fretwell, P., Pritchard, H.D., Vaughan, D.G., Bamber, J.L., Barrand, N.E., Bell, R., Bianchi, C.,
726 Bingham, R.G., Blankenship, D.D., Casassa, G., Catania, G., Callens, D., Conway, H., Cook, A.J.,
727 Corr, H.F.J., Damaske, D., Damm, V., Ferraccioli, F., Forsberg, R., Fujita, S., Gim, Y., Gogineni,
728 P., Griggs, J.A., Hindmarsh, R.C.A., Holmlund, P., Holt, J.W., Jacobel, R.W., Jenkins, A., Jokat,
729 W., Jordan, T., King, E.C., Kohler, J., Krabill, W., Riger-Kusk, M., Langley, K.A., Leitchenkov,
730 G., Leuschen, C., Luyendyk, B.P., Matsuoka, K., Mouginot, J., Nitsche, F.O., Nogi, Y., Nost, O.
731 A., Popov, S.V., Rignot, E., Rippin, D.M., Rivera, A., Roberts, J., Ross, N., Siegert, M.J., Smith,
732 A.M., Steinhage, D., Studinger, M., Sun, B., Tinto, B.K., Welch, B.C., Wilson, D., Young, D.A.,
733 Xiangbin, C., Zirizzotti, A., 2013. Bedmap2: Improved ice bed, surface and thickness datasets for
734 Antarctica. Cryosphere 7, 375-393.

735 Gradstein, F.M., Ogg, J.G., Schmitz, M.D., Ogg, G.M., 2012. The Geologic Time Scale 2012. The
736 Geologic Time Scale 2012 1-2, 1-1144.

737 Gradstein, F.M., Ogg, J.G., Smith, A.G., 2004. A geologic timescale 2004. Cambridge University
738 Press, Cambridge.

739 Greenop, R., Foster, G.L., Wilson, P.A., Lear, C.H., 2014. Middle Miocene climate instability
740 associated with high-amplitude CO_2 variability. Paleoceanography. 29, 845-853.

741 Hartman, J.D., Bijl, P.K., Sangiorgi, F., Peterse, F., Schouten, S., Salabarnada, A., Bohaty, S.,
742 Escutia, C., Brinkhuis, H. Oligocene TEX$_{86}$-derived sea surface temperatures from the Wilkes Land
743 Margin, Antarctica. Submitted, this volume.

744 Harwood, D., Levy, R., Cowie, J., Florindo, F., Naish, T., Powell, R., Pyne, A., 2006. Deep drilling
745 with the ANDRILL program in Antarctica. Scientific Drilling 1, 43-45.

746 Hauptvogel, D.W., Pekar, S.F., Pincay, V., 2017. Evidence for a heavily glaciated Antarctica
747 during the late Oligocene "warming" (27.8-24.5): stable isotope records from ODP Site 690.
748 Paleoceanography. PA002972, 384-384-396.

749 Herold, N., Huber, M., Müller, R.D., 2011. Modeling the Miocene Climatic Optimum. Part I: Land
750 and atmosphere. Journal of Climate 24, 6353-6373.

751 Herold, N., Huber, M., Müller, R.D., Seton, M., 2012. Modeling the Miocene Climatic Optimum:
752 Ocean circulation. Paleoceanography 27, PA1209.

753 Hill, D.J., Haywood, A.M., Valdes, P.J., Francis, J.E., Lunt, D.J., Wade, B.S., Bowman, V.C.,
754 2013. Paleogeographic controls on the onset of the Antarctic circumpolar current. Geophysical
755 Research Letters 40, 5199-5204.

756 Holbourn, A., Kuhnt, W., Kochhann, K.G.D., Andersen, N., Meier, K.J., 2015. Global perturbation
757 of the carbon cycle at the onset of the Miocene Climatic Optimum. Geology 43, 123-126.

758 Houben, A.J.P., 2012. Triggers and Consequences of glacial expansion across the Eocene-
759 Oligocene transition. LPP contributions series no. 39, PhD thesis Utrecht University, Utrecht, the
760 Netherlands.

761 Houben, A.J.P., Bijl, P.K., Pross, J., Bohaty, S.M., Passchier, S., Stickley, C.E., Röhl, U., Sugisaki,
762 S., Tauxe, L., Van De Flierdt, T., Olney, M., Sangiorgi, F., Sluijs, A., Escutia, C., Brinkhuis, H.,
763 2013. Reorganization of Southern Ocean plankton ecosystem at the onset of Antarctic glaciation.
764 Science 340, 341-344.

765 IPCC, 2013. Climate Change 2013: The Physical Science Basis. Contribution of Working Group I
766 to the Fifth Assessment Report of the Intergovernmental Panel on Climate Change. Cambridge
767 University Press, Cambridge, United Kingdom and New York, NY, USA.

Climate
of the Past

Discussions

Open Access

768 Knorr, G. and Lohmann, G., 2014. Climate warming during antarctic ice sheet expansion at the
769 middle miocene transition. Nature Geoscience 7, 376-381.

770 Kohfeld, K.E., Graham, R.M., de Boer, A.M., Sime, L.C., Wolff, E.W., Le Quéré, C., Bopp, L.,
771 2013. Southern Hemisphere westerly wind changes during the Last Glacial Maximum: paleo-data
772 synthesis. Quaternary Science Reviews. 68, 76-95.

773 Levy, R.H., Harwood, D.M., 2000. Tertiary marine palynomorphs from the McMurdo Sound
774 erratics, Antarctica, in: Stilwell, J. D., Feldmann, R. M. (Eds.), Paleobiology and
775 Paleoenvironments of Eocene rocks, McMurdo Sound, East Antarctica. AGU Antarctic Research
776 Series, pp. 183-242.

777 Liebrand, D., de Bakker, A.T.M., Beddow, H.M., Wilson, P.A., Bohaty, S.M., Ruessink, G.,
778 Pälike, H., Batenburg, S.J., Hilgen, F.J., Hodell, D.A., Huck, C.E., Kroon, D., Raffi, I., Saes, M.J.
779 M., van Dijk, A.E., Lourens, L.J., 2017. Evolution of the early Antarctic ice ages. PNAS 110(15),
780 3867-3867-3872.

781 Liebrand, D., Lourens, L.J., Hodell, D.A., De Boer, B., Van De Wal, R.S.W., Pälike, H., 2011.
782 Antarctic ice sheet and oceanographic response to eccentricity forcing during the early Miocene.
783 Climate of the Past 7, 869-880.

784 Olbers, D., Borowski, D., Völker, C., Wölff, J. -., 2004. The dynamical balance, transport and
785 circulation of the Antarctic Circumpolar Current. Antarctic Science 16, 439-470.

786 Pälike, H., Norris, R.D., Herrle, J.O., Wilson, P.A., Coxall, H.K., Lear, C.H., Shackleton, N.J.,
787 Tripati, A.K., Wade, B.S., 2006. The Heartbeat of the Oligocene Climate System. Science 314,
788 1894-1898.

789 Prebble, J.G., Crouch, E.M., Carter, L., Cortese, G., Bostock, H., Neil, H., 2013. An expanded
790 modern dinoflagellate cyst dataset for the Southwest Pacific and Southern Hemisphere with
791 environmental associations. Marine Micropaleontology 101, 33-48.

792 Rignot, E., Jacobs, S., Mouginot, J., Scheuchl, B., 2013. Ice-shelf melting around Antarctica.
793 Science 341, 266-270.

794 Robert, C., Anderson, J., Armienti, P., Atkins, C., Barrett, P., Bohaty, S., Bryce, S., Claps, M.,
795 Curran, M., Davey, F.J., De Santis, L., Ehrmann, W., Florindo, F., Fielding, C., Hambrey, M.,
796 Hannah, M., Harwood, D.M., Henrys, S., Hoelscher, F., Howe, J.A., Jarrard, R., Kettler, R.,
797 Kooyman, S., Kopsch, C., Krissek, L., Lavelle, M., Levac, E., Niessen, F., Passchier, S., Paulsen,
798 T., Powell, R., Pyne, A., Rafat, G., Raine, I. J., Roberts, A.P., Sagnotti, L., Sandroni, S., Scholz, E.,
799 Simes, J., Smellie, J., Strong, P., Tabecki, M., Talarico, F.M., Taviani, M., Verosub, K.L., Villa,
800 G., Webb, P.N., Wilson, G.S., Wilson, T., Wise, S.W., Wonik, T., Woolfe, K., Wrenn, J.H., 1998.
801 Summary of Results from CRP-1, Cape Roberts Project, Antarctica. Terra Antartica 5, 125-137.

802 Rovere, A., Raymo, M.E., Mitrovica, J.X., Hearty, P.J., O'Leary, M.J., Inglis, J.D., 2014. The Mid-
803 Pliocene sea-level conundrum: Glacial isostasy, eustasy and dynamic topography. Earth and
804 Planetary Science Letters 387, 27-33.

805 Salabarnada, A., Escutia, et. al., Lithology of Oligocene of U1356. Submitted, this volume.

806 Sangiorgi, F., Bijl, P.K., Passchier, S., Salzmann, U., Schouten, S., McKay, R., Cody, R.D., Pross,
807 J., vd Flierdt, T., Bohaty, S. M., Levy, R., Williams, T., Escutia, C., Brinkhuis, H., Warm Southern
808 Ocean linked to a reduced size of the East Antarctic ice sheet during the mid Miocene. In review,
809 Nature communications.

810 Scher, H.D. and Martin, E.M., 2004. Circulation in the Southern Ocean during the Paleogene
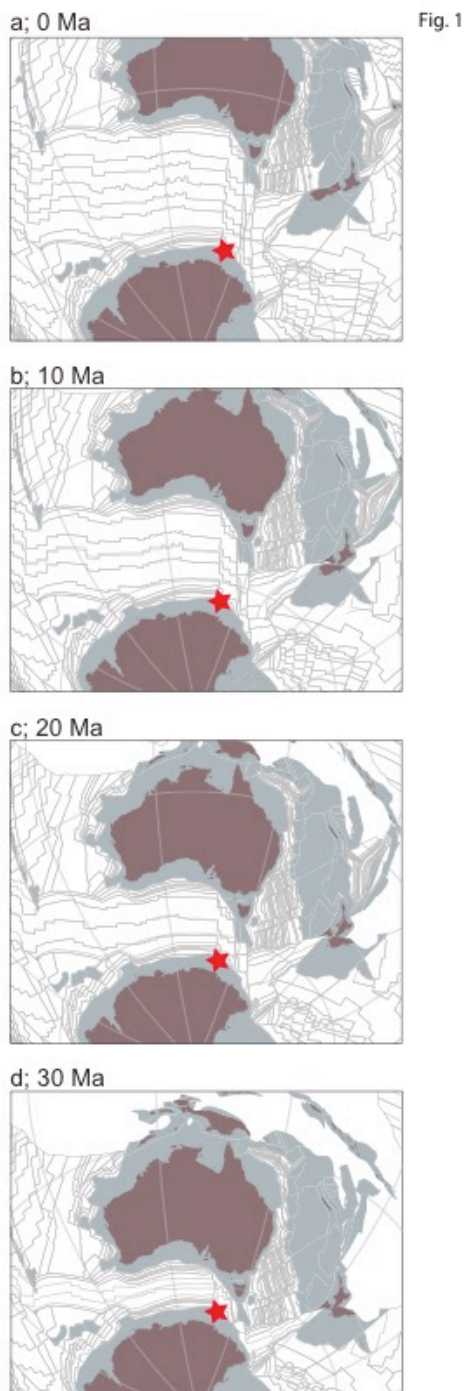811 inferred from neodymium isotopes. Earth and Planetary Science Letters 228, 391-405.

812   Scher, H.D., Whittaker, J.M., Williams, S.E., Latimer, J.C., Kordesch, W.E.C., Delaney, M.L.,
813   2015. Onset of Antarctic Circumpolar Current 30 million years ago as Tasmanian Gateway aligned
814   with westerlies. Nature 523, 580-583.

815   Seton, M., Müller, R.D., Zahirovic, S., Gaina, C., Torsvik, T., Shephard, G., Talsma, A., Gurnis,
816   M., Turner, M., Maus, S., Chandler, M., 2012. Global continental and ocean basin reconstructions
817   since 200Ma. Earth-Science Reviews 113, 212-270.

818   Shepherd, A., Ivins, E.R., Geruo, A., Barletta, V.R., Bentley, M.J., Bettadpur, S., Briggs, K.H.,
819   Bromwich, D.H., Forsberg, R., Galin, N., Horwath, M., Jacobs, S., Joughin, I., King, M.A.,
820   Lenaerts, J.T.M., Li, J., Ligtenberg, S.R.M., Luckman, A., Luthcke, S.B., McMillan, M., Meister,
821   R., Milne, G., Mouginot, J., Muir, A., Nicolas, J.P., Paden, J., Payne, A.J., Pritchard, H., Rignot,
822   E., Rott, H., Sørensen, L.S., Scambos, T.A., Scheuchl, B., Schrama, E.J.O., Smith, B., Sundal, A.
823   V., Van Angelen, J.H., Van De Berg, W.J., Van Den Broeke, M.R., Vaughan, D.G., Velicogna, I.,
824   Wahr, J., Whitehouse, P. L., Wingham, D.J., Yi, D., Young, D., Zwally, H.J., 2012. A reconciled
825   estimate of ice-sheet mass balance. Science 338, 1183-1189.

826   Sluijs, A., Brinkhuis, H., Stickley, C.E., Warnaar, J., Williams, G.L., Fuller, M., 2003.
827   Dinoflagellate cysts from the Eocene - Oligocene transition in the Southern Ocean: Results from
828   ODP Leg 189, in: Exon, N., Kennett, J. P. (Eds.), Proceedings of the Ocean Drilling Program,
829   Scientific Results, volume 189. U.S. Government Printing Office, College Station, Texas, USA.

830   Sluijs, A., Pross, J., Brinkhuis, H., 2005. From greenhouse to icehouse; organic walled
831   dinoflagellate cysts as paleoenvironmental indicators in the Paleogene. Earth-Science Reviews. 68,
832   281-315.

833   Strother, S.L., Salzmann, U., Sangiorgi, F., Bijl, P.K., Pross, J., Escutia, C., Salabarnada, A.,
834   Pound, M.J., Voss, J., Woodward, J., 2017. A new quantitative approach to identify reworking in
835   Eocene to Miocene pollen records from offshore Antarctica using red fluorescence and digital
836   imaging. Biogeosciences. 14, 2089-2100.

837   Tauxe, L., Stickley, C.E., Sugisaki, S., Bijl, P.K., Bohaty, S., Brinkhuis, H., Escutia, C., Flores, J.
838   A., Iwai, M., Jimenez-Espejo, F., McKay, R., Passchier, S., Pross, J., Riesselman, C., Röhl, U.,
839   Sangiorgi, F., Welsh, K., Klaus, A., Bendle, J.A.P., Dunbar, R., Gonzalez, J., Olney, M.P., Pekar,
840   S.F., van de Flierdt, T., 2012. Chronostratigraphic framework for the IODP Expedition 318 cores
841   from the Wilkes Land Margin: constraints for paleoceanographic reconstruction. Paleoceanography
842   27, PA2214.

843   Torsvik, T.H., Van der Voo, R., Preeden, U., Niocaill, C.M., Steinberger, B., Doubrovine, P.V.,
844   van Hinsbergen, D.J.J., Domeier, M., Gaina, C., Tohver, E., Meert, J.G., McCausland, P.J., Cocks,
845   L.R.M., 2012. Phanerozoic polar wander, palaeogeography and dynamics. Earth-Science Reviews
846   114, 325-368.

847   Van Hinsbergen, D.J.J., De Groot, L.V., Van Schaik, S.J., Spakman, W., Bijl, P.K., Sluijs, A.,
848   Langereis, C.G., Brinkhuis, H., 2015. A paleolatitude calculator for paleoclimate studies. PLoS
849   ONE 10(6): e0126946

850   Wilson, G.S., Bohaty, S.M., Fielding, C.R., Florindo, F., Hannah, M.J., Hardwood, D.M.,
851   Mcintosh, W.C., Naish, T.R., Roberts, A.P., Sagnotti, L., Scherer, R.P., Strong, C.P., Verosub,
852   K.L., Villa, G., Webb, P. -., Woolfe, K. J., 2000. Chronostratigraphy of CRP-2/2A, Victoria Land
853   Basin, Antarctica. Terra Antarctica 7, 647-654.

854   Wise, S.W., Schlich, R., 1992. Proceedings of the Ocean Drilling Program, Scientific Results,
855   volume 120. U.S. Government Printing Office, College Station, Texas.

856   Wouters, B., Martin-Español, A., Helm, V., Flament, T., van Wessem, J.M., Ligtenberg, S.R.M.,
857   van den Broeke, M.R., Bamber, J.L., 2015. Dynamic thinning of glaciers on the Southern Antarctic
858   Peninsula. Science 348 (6237), 899-903.
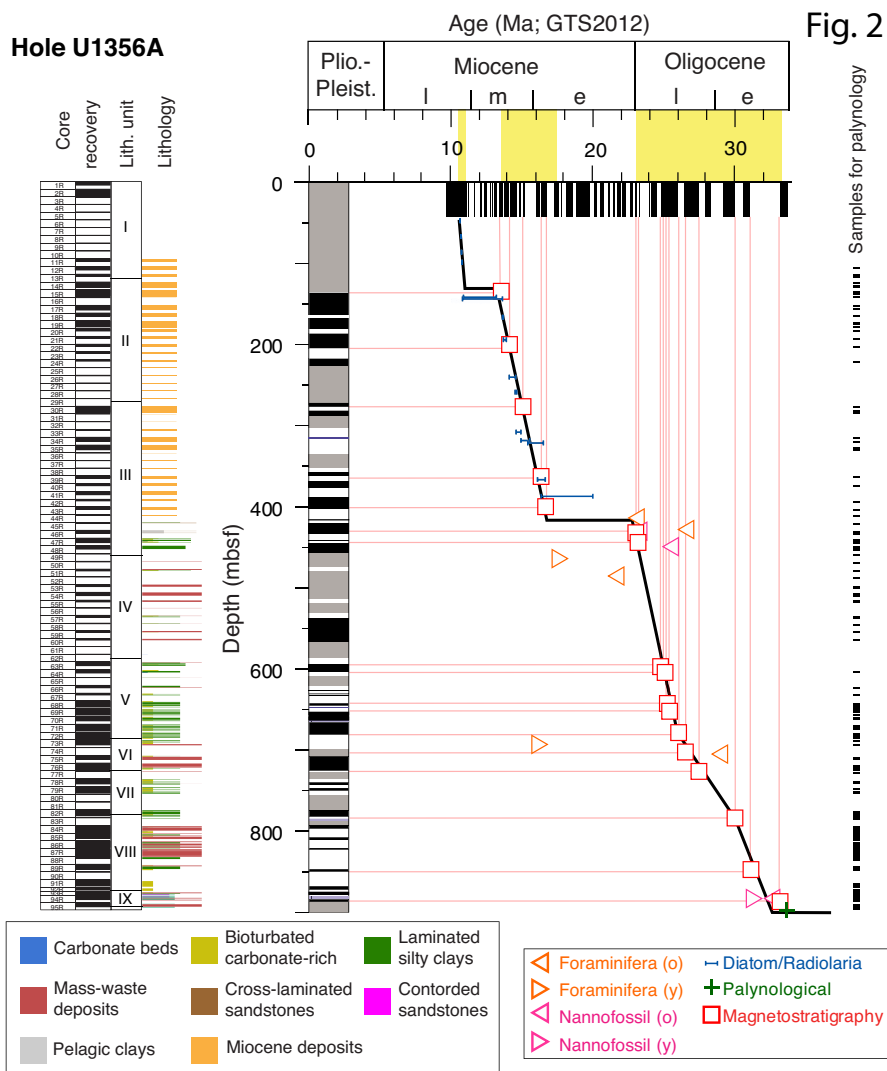
Climate
of the Past

Discussions

859   Wrenn, J.H. and Hart, G.F., 1988. Paleogene dinoflagellate cyst biostratigraphy of Seymour Island,
860   Antarctica. Geological Society of America Memoires 169, 321-447.

861   Zachos, J.C., Dickens, G.R., Zeebe, R.E., 2008. An early Cenozoic perspective on greenhouse
862   warming and carbon-cycle dynamics. Nature 451, 279-283.

863   Zevenboom, D., 1995. Dinoflagellate cysts from the Mediterranean late Oligocene and Miocene.
864   PhD thesis Utrecht University, Utrecht, the Netherlands

865   Zonneveld, K.A.F., Marret, F., Versteegh, G.J.M., Bogus, K., Bonnet, S., Bouimetarhan, I.,
866   Crouch, E., de Vernal, A., Elshanawany, R., Edwards, L., Esper, O., Forke, S., Grøsfjeld, K.,
867   Henry, M., Holzwarth, U., Kielt, J., Kim, S., Ladouceur, S., Ledu, D., Chen, L., Limoges, A.,
868   Londeix, L., Lu, S., Mahmoud, M.S., Marino, G., Matsouka, K., Matthiessen, J., Mildenhal, D.C.,
869   Mudie, P., Neil, H.L., Pospelova, V., Qi, Y., Radi, T., Richerol, T., Rochon, A., Sangiorgi, F.,
870   Solignac, S., Turon, J., Verleye, T., Wang, Y., Wang, Z., Young, M., 2013. Atlas of modern
871   dinoflagellate cyst distribution based on 2405 data points. Review of Palaeobotany and Palynology
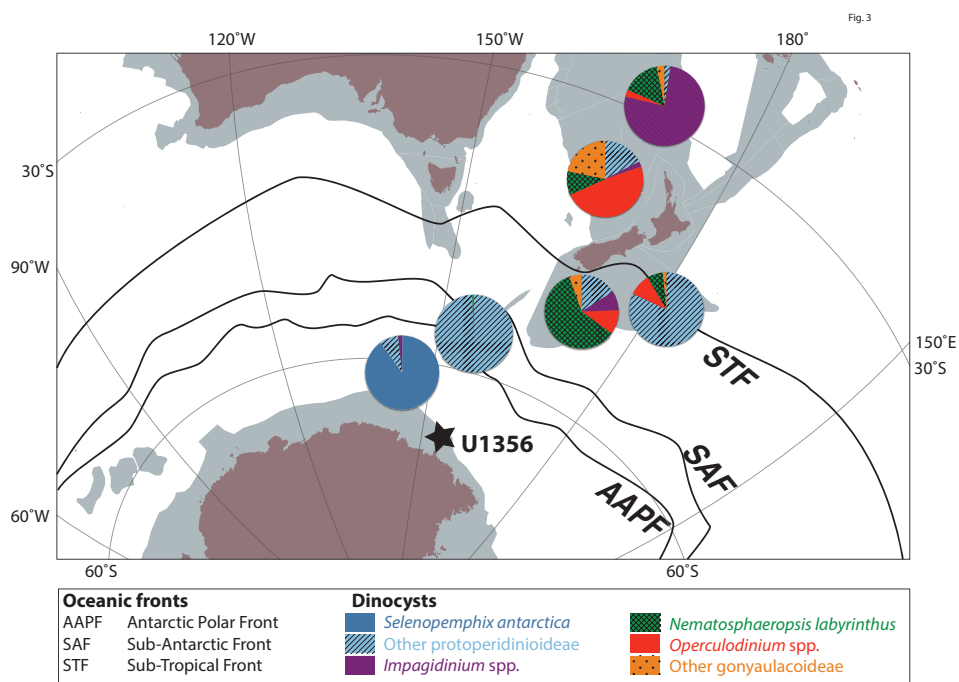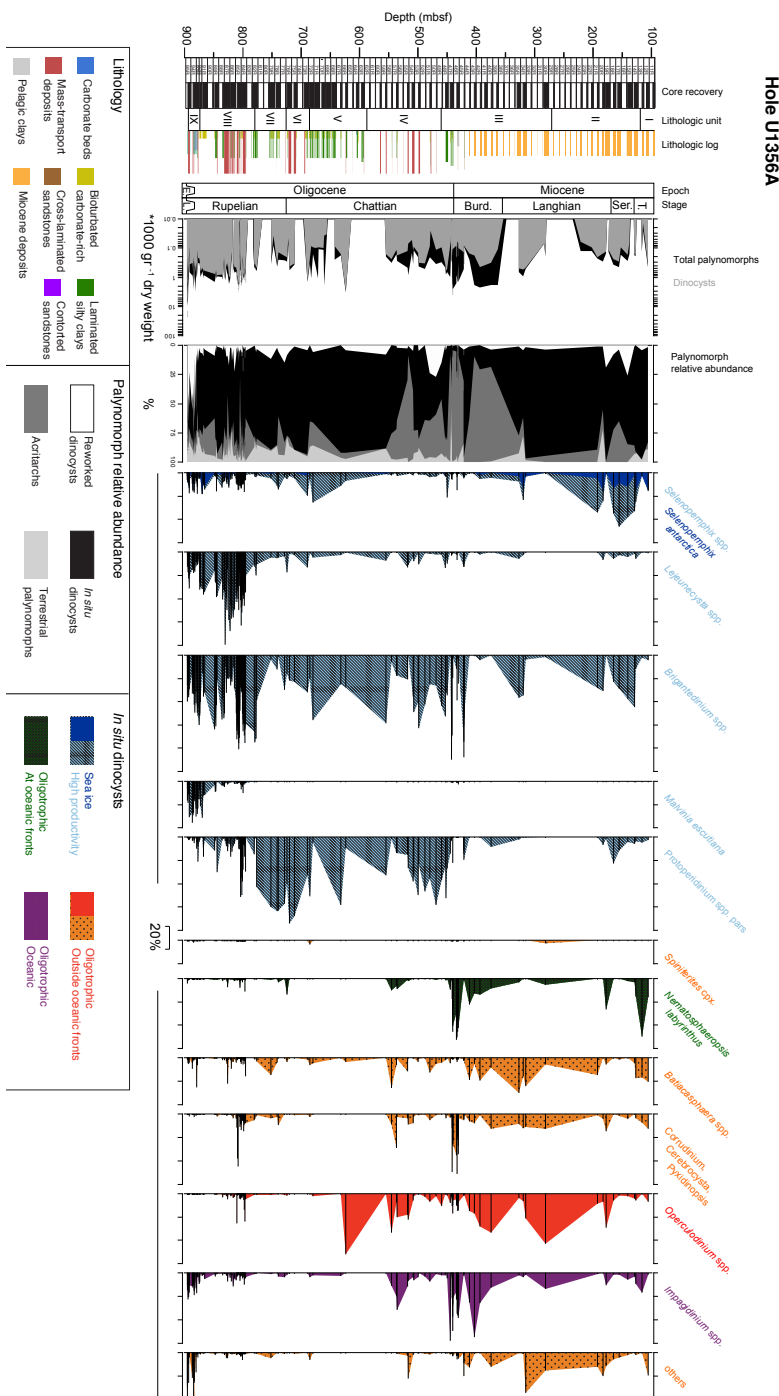872   191, 1-197.

873

Fig. 1

874

875

Fig. 2

Oceanic fronts

AAPF	Antarctic Polar Front
SAF	Sub-Antarctic Front
STF	Sub-Tropical Front

Dinocysts

Selenopemphix antarctica
Other protoperidinioideae
Impagidinium spp.
Nematosphaeropsis labyrinthus
Operculodinium spp.
Other gonyaulacoideae

878

879

Fig. 5

Fig. 6

936

937

Fig. 7

Climate
of the Past
Discussions
Open Access
EGU

Table 1
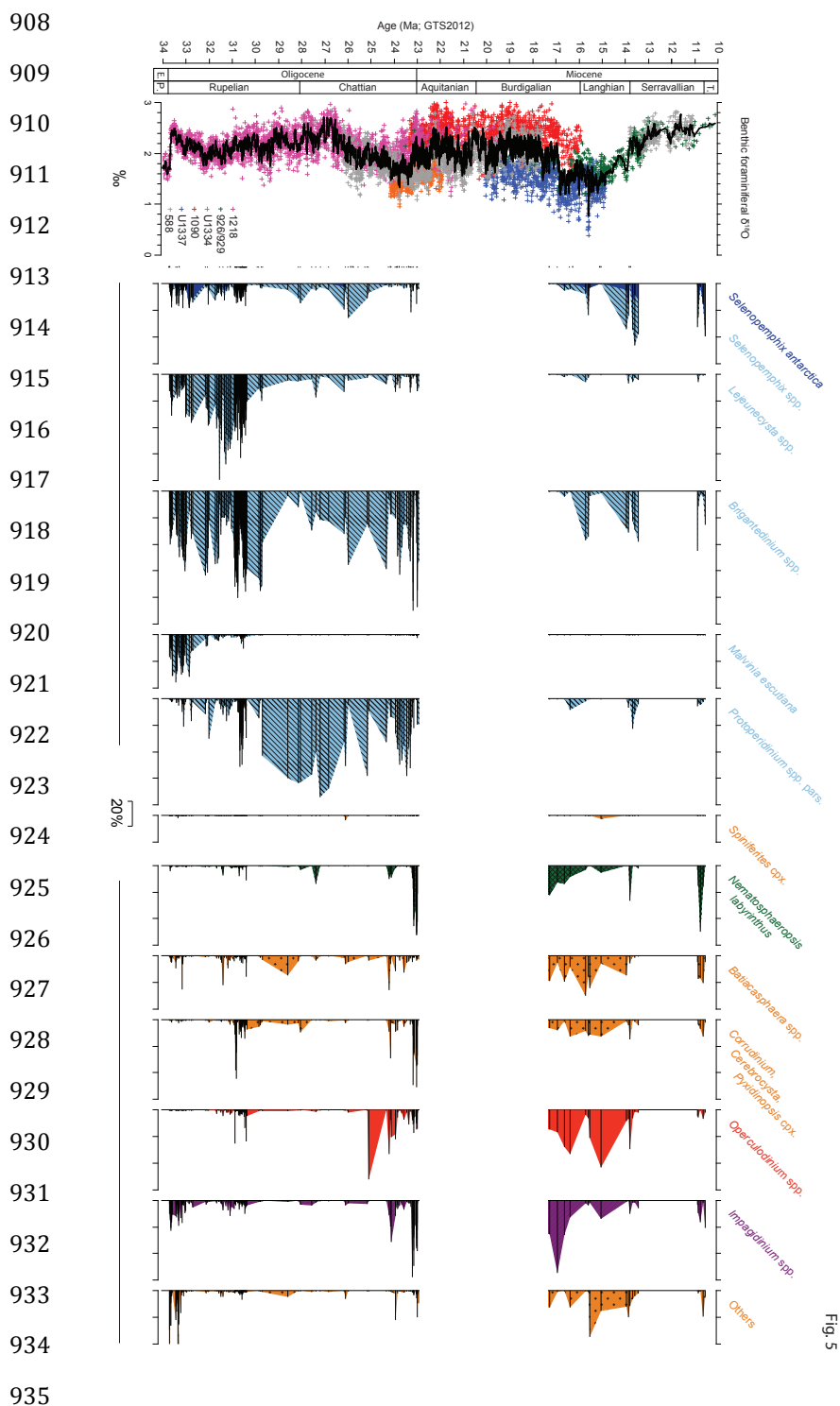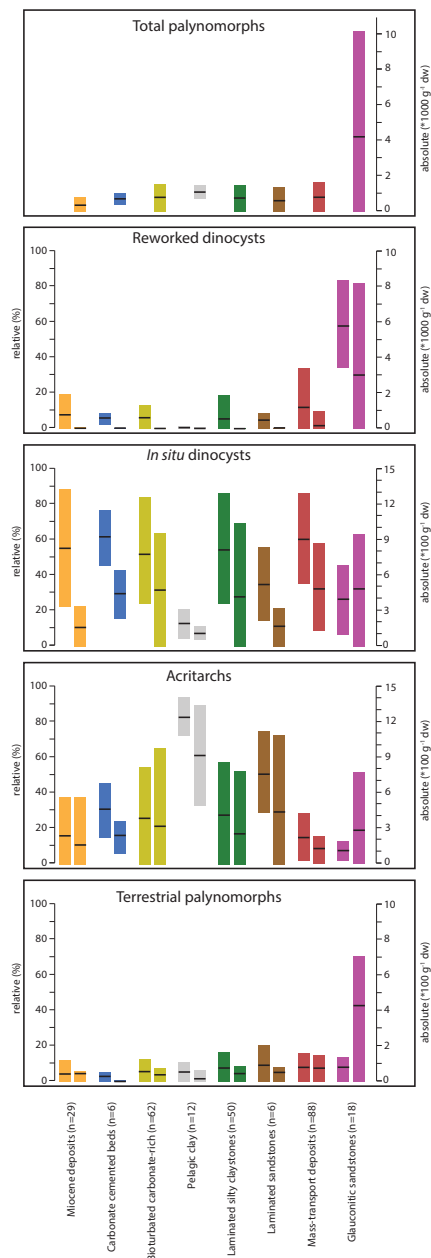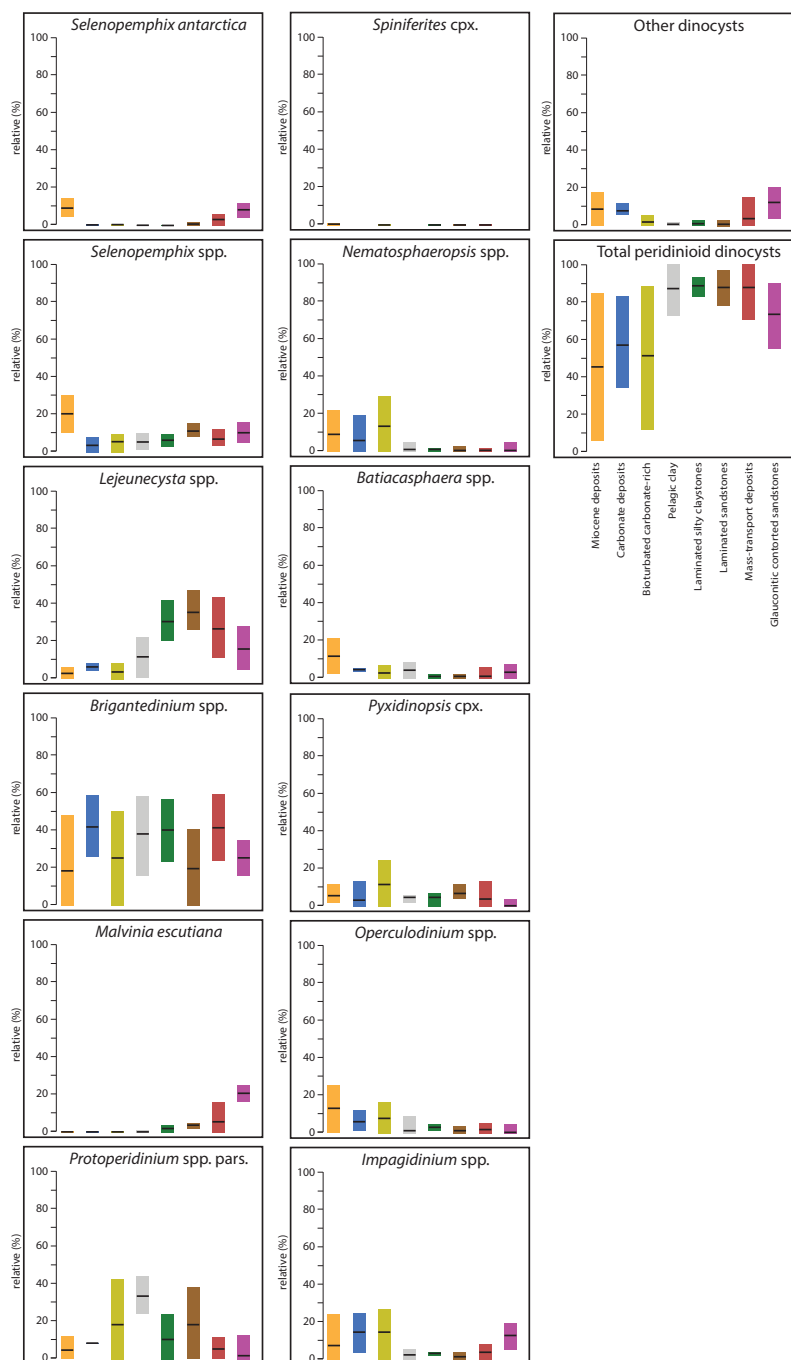
type	FO/LO	Genus, chron	Gradstein 2012	top core	top interval	bottom core	bottom interval	depth average	error
CONOP			10.76					98.66	
CONOP			10.92					133.80	
CONOP			13.41					133.81	
PM	(o)	C5ACn	14.07	22R-2,	75	22R-2,	90	203.23	0.07
PM	(y)	C5Bn.2n	15.03	30R-2,	50	30R-2,	75	279.63	0.13
PM	(o)	C5Cn.1n	16.27	39R-1,	35	39R-1,	65	364.10	0.15
PM	(o)	C5Cn.3n	16.72	42R-2,	59	43R-1,	25	398.28	3.98
			17.50	44R-CC		45R-CC		416.90	
			23.00	44R-CC		45R-CC		416.91	
PM	(o)	C6Cn.2n	23.03	45R-CC	40	46R-1	65	426.78	5.00
PM	(o)	C6Cn.3n	23.30	50R-1,	0			469.00	9.00
PM	(y)	C7An	24.76	63R-3,	85	63R-3,	120	597.12	0.17
PM	(o)	C7An	24.98	64R-1,	130	64R-1,	135	604.33	0.02
PM	(o)	C8n.1n	25.26	68R-2,	20	68R-2,	75	643.38	0.27
PM	(y)	C8n.2n	25.30	69R-2,	20	69R-2,	25	652.58	0.02
PM	(o)	C8n.2n	25.99	71R-6,	115	72R-1,	10	678.98	0.92
PM	(y)	C9n	26.42	73R-4,	90	75R-1,	15	701.66	7.09
PM	(o)	C9n	27.44	76R-6,	35	76R-6,	40	725.09	0.02
PM	(o)	C11n.2n	29.97	82R-6,	35	82R-6,	40	782.68	0.03
PM	(y)	C13n	33.16	93R-1,117		93R-2,	28	878.00	0.23

940

Table 2

in Salabarnada et al. (submitted this volume)	in this paper
Laminated facies "F1"	Laminated siltstones
	Laminated sandstones
Bioturbated facies "F2"	Bioturbated carbonate-rich
	Pelagic clays
Carbonate cemented beds	Carbonate cemented beds
Turbidites and hemipelagites	Miocene deposits
Slumps facies	
Debris flows facies	Mass-waste deposits
EOT facies	
Eocene sands facies	Glauconite sandstones

941

942

Climate
of the Past
Discussions

Table 3

In situ taxa	Reworked taxa
Adnatosphaeridium? sp.	*Achilleodinium biformoides*
Ataxodinium choane	*Achomosphaera alcicornu*
Batiacasphaera compta	*Aiora fenestrata*
Batiacasphaera spp. (pars.)	*Aireiana verrucosa*
Batiacasphaera hirsuta	*Adnatosphaeridium* spp.
Batiacasphaera micropapillata	*Alisocysta circumtabulata*
Batiacasphaera minuta	*Alterbidinium distinctum*
Batiacasphaera sphaerica	*Apectodinium* spp.
Batiacasphaera sp. A	*Arachnodinium antarcticum*
Batiacasphaera sp. B	*Areoligera* spp. (pars)
Batiacasphaera sp. C	*Areoligera semicirculata*
Batiacasphaera sp. D	*Cerebrocysta bartonensis*
Brigantedinium simplex	*Charlesdowniea clathrata*
Brigantedinium pynei	*Charlesdowniea edwardsii*
Brigantedinium sp. A	*Cooksonidinium capricornum*
Brigantedinium sp. B	*Cordosphaeridium fibrospinosum*
Brigantedinium sp. C	*Cordosphaeridium funiculatum*
Brigantedinium sp. D	*Corrudinium incompositum*
Cerebrocysta WR small	*Corrudinium regulare*
Cerebrocysta delicata	*Cribroperidinium* spp.
Cerebrocysta sp. A	*Damassadinium crassimuratum*
Cleistosphaeridium sp. B	*Dapsilidinium* spp.
Cleistosphaeridium sp.A	*Deflandrea* sp. A sensu Brinkhuis et al., 2003
Cordosphaeridium minutum	*Deflandrea antarctica*
Corrudinium labradori	*Deflandrea cygniformis*
Corrudinium sp. A	*Diphyes colligerum*
Cryodinium? sp.	*Deflandrea* spp. Indet
Distatodinium spp.	*Eisenackia circumtabulata*
Edwardsiella sexispinosa	*Enneadocysta diktyostila*
Elytrocysta sp. A	*Enneadocysta multicornuta*
Elytrocysta brevis	*Eocladopyxis tesselata*
Gelatia inflata	*Fibrocysta axialis*
Habibacysta? spp.	*Glaphyrocysta intricta*
Homotryblium spp.	*Glaphyrocysta pastielsii*
Hystrichokolpoma bullatum	*Heteraulacacysta leptalea*
Huystrichosphaeropsis obscura	*Histiocysta palla*
Impagidinium spp. (pars)	*Hystrichokolpoma pusilla*
Impagidinium aculeatum	*Hystrichokolpoma rigaudiae*
Impagidinium cantabrigiense	*Hystrichokolpoma truncatum*
Impagidinium elegans	*Hystrichosphaeridium truswelliae*
Impagidinium elongatum	*Hystrichosphaeridium tubiferum*
Impagidinium pacificum	*Impagidinium maculatum*
Impagidinium pallidum	*Impagidinium waipawense*
Impagidinium paradoxum	*Kenleyia* spp.
Impagidinium patulum	*Manumiella druggii*
Impagidinium plicatum	*Melitasphaeridium pseudorecurvatum*
Impagidinium velorum	*Membranophoridium perforatum*
Impagidinium victorianum	*Octodinium askiniae*
Impagidinium sp. A	*Odontochitina* spp.
Impagidinium sphaericum	*Operculodinium* spp.
Invertocysta tabulata	*Phthanoperidinium antarcticum*
Islandinium spp.	*Phthanoperidinium echinatum*
Lejeunecysta attenuata	*Polysphaeridium* spp.
Lejeunecysta adeliense	*Rhombodinium* sp.
Lejeunecysta fallax	*Schematophora speciosa*
Lejeunecysta cowei	*Schematophora obscura*
Lejeunecysta acuminata	*Senegalinium* spp.
Lejeunecysta rotunda	*Spinidinium luciae*
Lejeunecysta katatonos	*Spinidinium macmurdoense*
Malvinia escutiana	*Spinidinium schellenbergii*
Nematosphaeropsis labyrinthus	*Spiniferites ramosus* CPX
Oligokolpoma galeotti	*Thalassiphora pelagica*
Operculodinium tiara	*Turbiosphaera filosa*
Operculodinium sp. A	*Turbiosphaera sagena*
Operculodinium piaseckii	*Vozzhennikovia apertura/ S.schellenbergii* group
Operculodinium janduchenei	*Vozzhennikovia netrona*
Operculodinium cf *eirikianum*	*?Vozzhenikovia* LARGE
Operculodinium eirikianum	*Wetzeliella articulata*
Paleocystodinium golzowense	
Paucisphaeridium spp.	
Phthanoperidinium amoenum	
Pyxidinopsis spp. (pars)	
Pyxidinopsis sp. A	
Pyxidinopsis sp. B	
Pyxidinopsis sp. C	
Pyxidinopsis sp. D	
Pyxidinopsis vesciculata	
Pyxidinopsis tuberculata	
Pyxidinopsis reticulata	
Pyxidinopsis fairhavensis	
Reticulatosphaera actinocoronata	
Selenopemphix antarctica	
Selenopemphix nephroides	
Selenopemphix dioneacysta	
Selenopemphix sp. A	
Selenopemphix undulata	
Selenopemphix brinkhuisi	
Spiniferites sp. B	
Spiniferites sp. A	
Spiniferites sp. C	
Stoveracysta ornata	
Stoveracysta kakanuiensis	
?Svalbardella spp.	
Tectatodinium spp.	
Unipontedinium aquaeductus	
Protoperidinioid indet	
Protoperidinium sp. B	
Protoperidinium sp. A	
Protoperidinium sp. C	
Protoperidinium sp. D	

943